Journal of Manufacturing Processes 44 (2019) 91–101

Contents lists available at ScienceDirect

Journal of Manufacturing Processes

journal homepage: www.elsevier.com/locate/manpro

Experimental investigation of phase change materials fabricated using selective laser sintering additive manufacturing

Malek Nofal[a], Said Al-Hallaj[b], Yayue Pan[a,*]

[a] University of Illinois at Chicago, 842 W Taylor Street, Chicago, IL, 60607, United States
[b] AllCell Technologies, 2321 W 41st Street, Chicago, IL, 60609, United States

ARTICLE INFO

Keywords:
3D printing
Selective laser sintering
Phase change material
Paraffin-graphite composite
Self bonding

ABSTRACT

The increased demand for phase-change-materials-enabled energy storage systems exposed the limitations of established manufacturing methods in terms of material properties, fabrication speed, material waste, and shape-form flexibility. Phase change materials have unique merits in latent heat thermal energy storage, due to its capability of providing high-energy density storage by solidifying/melting at a constant temperature. In this research, a phase change composite was developed by mixing paraffin wax with a thermal conductive expanded graphite. Using a layer-by-layer laser sintering method, these two materials were combined at a micro-scale, forming a phase change composite that possesses good thermal conductivity, superior latent heat, and good mechanical strength. This work investigated the key parameters for successful production of paraffin wax/expanded graphite composite using laser sintering technique. In particular, the paraffin wax is melted and then impregnated into the inter-particle pores of expanded graphite through capillaries. It serves as a binder that bonds the expanded graphite molecules together into a solid form-stable object during the laser sintering process. To validate the developed sintering process, samples with a various number of layers were fabricated and tested. Results showed good structural integrity and functionality of the printed samples. The thermal conductivity was in the range of 0.83–0.92 $W\,m^{-1}\,K^{-1}$. The latent heat was in the range of 150–156 $kJ\,kg^{-1}$. Modulus of elasticity was between 808–880 MPa while the tensile strength in the range of 2.2–3.3 MPa. The electrical resistivity ranged between 8 and 28 Ohm m. These experimental results verified that the developed laser sintering process could be used as an effective nontraditional manufacturing technique for fabricating phase change materials for thermal energy storage applications.

1. Introduction

1.1. Background

Lithium-ion batteries energy density has doubled in the last decade. This allows for more compact and efficient battery-powered goods such as electric vehicles, drones, portable electronics, and renewable energy storage. However, the high-energy density comes with a price of properly maintaining a safe operation of such batteries. The heat generated during charging and discharging might lead to life cycle degradation and severe thermal runaway. Therefore, integrating lithium-ion batteries with a mean of cooling mechanism has been a common practice in high power applications. Passive cooling mechanisms which can be achieved by using phase change materials (PCM) has gotten a lot of attention lately.

Phase change materials have become game changers in modern thermal energy application. Due to the phenomenon of state change in phase, i.e. solid-liquid or liquid-gas phase change, thermal energy can be stored and extracted in the form of latent heat. The liquid-gas phase change provides a huge amount of latent heat [1]. However, the major drawback of such phase change scheme is the massive volume required to contain the gaseous phase. Therefore, the solid-liquid phase change has been considered a better approach and investigated in many literatures.

The key benefit of solid-liquid phase change materials is the high latent heat to sensible heat ratio, where the thermal energy can be stored without significantly increasing the phase change material temperature beyond its melting point. This advantage allows a uniform thermal heat absorption or extraction throughout the system.

For thermal energy storage applications that need to store the thermal energy at a fast rate, the thermal conductivity is a major property that needs to be taken into account. Other properties including

* Corresponding author.
E-mail addresses: mnofal2@uic.edu (M. Nofal), salhallaj@allcelltech.com (S. Al-Hallaj), yayuepan@uic.edu (Y. Pan).

https://doi.org/10.1016/j.jmapro.2019.05.043
Received 6 April 2018; Received in revised form 7 May 2019; Accepted 31 May 2019
Available online 06 June 2019

Nomenclature

SLS	Selective laser sintering
AM	Additive manufacturing
PCM	Phase change material
$Q_{EG,PW}$	Heat transfer path from expanded graphite to paraffin wax
$Q_{EG,EG}$	Heat transfer path within expanded graphite particles
$Q_{PW,EG}$	Heat transfer path from paraffin wax to expanded graphite
$Q_{PW,PW}$	Heat transfer path within paraffin particles
$C_{p,EG}$	Specific heat capacity of expanded graphite in ($kJ\,kg^{-1}\,K^{-1}$)
$C_{p,PW}$	Specific heat capacity of paraffin wax in ($kJ\,kg^{-1}\,K^{-1}$)
X_{EG}	Mass fraction percentage of expanded graphite
X_{PW}	Mass fraction percentage of paraffin wax
k	Thermal conductivity in ($W\,m^{-1}\,K^{-1}$)
ρ	is the mass density in ($kg\,m^{-3}$)
α	Thermal diffusivity in ($mm^2\,s^{-1}$)
DSC	Differential scanning calorimeter

mechanical strength and form stability, which is the ability to contain the liquid phase of the phase change material within the structure without leakage, must also be considered. Nevertheless, most phase change materials have poor thermal conductivities comparing to metallic materials such as copper or aluminum. Paraffin wax, for instance, has a thermal conductivity around $0.20\,W\,m^{-1}\,K^{-1}$ comparing to $385\,W\,m^{-1}\,K^{-1}$ and $205\,W\,m^{-1}\,K^{-1}$ for copper and aluminum respectively [2]. Therefore, many researchers have investigated methods of combining phase change materials with various thermally conductive materials. Sari et al. [3,4] have studied a different combination of paraffin wax - as a phase change material, with expanded graphite and high-density polyethylene (HDPE) aiming to enhance the thermal conductivity of the composites. Fang et al. [5] considered a paraffin boron nitride nanomaterial composites due to its superior thermal conductivity, which is ranging between 1700–2000 $W\,m^{-1}\,K^{-1}$ [6].

In this paper, paraffin wax was selected as a phase change material due to its superior stability during phase change, relatively high latent heat capacity, a wide range of melting temperatures, and its low cost and commercial availability. Expanded graphite was selected as the form stable matrix due to its superior properties such as lightweight, relatively high thermal conductivity and its commercial availability [7–9].

1.2. Challenges and contribution

Natural graphite structure is based on parallel sheets of carbon that are held by strong covalent bonds within a two-dimensional layer, forming a hexagonal pattern, while the stacked sheets are held together by weak van der Waals bonds [10]. This complex structure makes it difficult or nearly impossible to break the covalent bonds at a single-layer level. However, in reaction with acids such as sulfuric and nitric, and some heat treatments, the weak van der Waals bonds can break by some materials, such as the paraffin wax. The capability of breaking the van der Waals bonds allows the paraffin wax to be impregnated into the expanded graphite molecule.

To fabricate form-stable composite, many researchers have suggested compacting expanded graphite and immersing it in a bath of molten paraffin wax for a certain amount of time ranging from a few minutes to up to 12 h [1,4,7,11]. The immersion time depends on the part geometry and desired properties. After the bath immersion, the part is then machined to form the final geometry. Such process is time-consuming and difficult to fabricate composite with accurate wax filling ratio and filling pattern, and in some instances, making a material waste up to 90% in volume in the immersion step and the machining step.

Additive manufacturing, also known as 3D Printing, is a class of new technologies that fabricate a three-dimensional object by accumulating materials, usually from bottom to the top, in a layer-by-layer fashion. Additive manufacturing offers multiple advantages over traditional manufacturing techniques, including almost near zero material waste, reduced time to market, and construction of structures not possible with traditional manufacturing processes. Therefore, this paper investigates an additive manufacturing technique, Selective Laser Sintering (SLS), for fabricating paraffin wax/expanded graphite composite, to achieve the desired functionalities while free of geometry constraints and material waste. Despite the efforts in laser sintering of graphite-based composites, successful selective laser sintering of paraffin wax/expanded graphite composite has not been reported yet. Expanded graphite and paraffin wax have very different thermal behaviors and mass densities. Selective laser sintering of such two very dissimilar materials to make a functional and form-stable composite is very challenging.

In our study, instead of using binders, the paraffin wax is melted in such a way that the capillary force of the molten wax allows it to embed inside the expanded graphite molecule and bind expanded graphite together. To illustrate the process, Fig. 1 demonstrates the selective laser sintering process of paraffin wax/expanded graphite at the

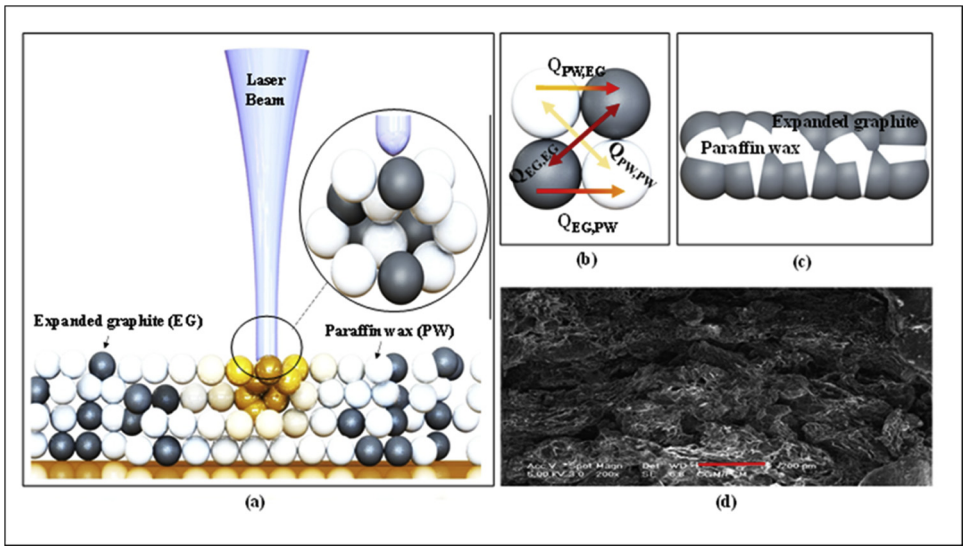

Fig. 1. Demonstration of paraffin wax/expanded graphite selective laser sintering process. (b) Four scenarios of heat transfer between particles; $Q_{EG,PW}$, $Q_{PW,EG}$, $Q_{EG,EG}$, and $Q_{PW,PW}$. (c) Paraffin wax/expanded graphite composite configuration after the laser sintering. (d) SEM illustration of the impregnated paraffin wax inside the expanded graphite matrix [7].

particle level. White spheres represent the paraffin wax, while the black spheres represent the expanded graphite. The molten paraffin wax impregnates into the micro-pores of expanded graphite molecules within the melting pool under the capillary force and bonds graphite particles together after it solidifies. In Fig. 1, during the sintering process, $Q_{EG,PW}$ is the heat transfer due to conduction from the expanded graphite to the paraffin wax while $Q_{PW,EG}$ is vice versa. $Q_{EG,EG}$ is the heat transfer within the expanded graphite particles while $Q_{PW,PW}$ is for paraffin wax. It is important to point out that expanded graphite and paraffin wax have significantly different thermal conductivities by three orders of magnitude. This affects the heat transfer rate between particles, making the selective laser sintering process challenging. Therefore, precise control over the particle size, composition, scan speed, output laser power, etc., is required to ensure adequate bonding and predictable heat transfer scheme between the particles. Accordingly, in this paper, experimental studies and sample characterizations were performed to address those challenges and develop the manufacturing process for successfully fabricating functional paraffin wax/expanded graphite composites, with desired properties.

The experiential setup is presented in Section 2.1, followed by materials preparations in Section 2.2, and the manufacturing process in Section 2.3. In Sections 3.2 and 3.3, thermal properties of the laser sintered samples are discussed, including the thermal conductivity and latent heat, which are critical properties in thermal energy storage applications. To test the form stability of the fabricated composites, mechanical properties such as the ultimate tensile strength and modulus of elasticity were characterized in Section 3.4. Additionally, to assess the functionality of the printed composite in electronics packing applications, the electrical resistivity of the sintered composite was characterized in Section 3.5. Discussion of the functionality of the selective laser sintered paraffin wax/graphite composite is given in Section 3.6, by comparing with the properties of existing phase change composite materials used in thermal storage applications. Finally, conclusion and future work are presented in Section 4.

2. Experimental study

2.1. Experimental setup

To examine the selective laser sintering technique for fabricating paraffin wax/expanded graphite composite, a testbed was constructed, as shown in Fig. 2. It consists of a constant wave (CW) laser module with a 445 nm wavelength and a 5.5 W output. The module is equipped with a constant-current driver board, ensuring a stable output laser power. The scan speed is in the range of 1.5–50 mm s^{-1}. A motorized linear stage XN10-0060-E01-71 from Velmex, Inc (Bloomfield, NY) was used as a Z-stage for layer-by-layer fabrication with an accuracy of 0.001" and repeatability of 0.0001". An aluminum platform (dimensions: 215 × 115 × 3 mm) was attached and leveled to the linear stage.

Table 1
Laser sintering parameters used in the experimental setup.

Parameter	Value
Output laser power	5.5 W
Laser wavelength	445 nm (blue laser)
Laser scan speed	1.5–50 mm s^{-1}
Scan spacing	0.25 mm
Deposition bed temperature	20 °C

Table 1 summarizes the parameters used in this experimental work.

Compared to long wavelength lasers such as IR laser, 445 nm laser generates lower heat power in the focal spot and hence allows more flexibility to adjust the scan speed and to control the melting pool and the composite formation process. The paraffin wax used in this study has a low melting point (~55 °C). Thus, long wavelength lasers can easily cause over-fast melting or undesirably large melting pools.

2.2. Material preparation

Particle size, mixture uniformity, and layer thickness are critical parameters in the selective laser sintering process [12]. Expanded graphite flakes from Superior Graphite (Chicago, IL) and paraffin wax from IGI (Titusville, PA) were used. The expanded graphite was in a fluffy and vermicular form, and the paraffin wax comes in a block form as shown in Fig. 3. In this work, both materials were processed in order to produce fine and uniform particles for sintering. Due to its low-density nature, expanded graphite was ground using low-speed ball milling apparatus 3A from Lortone (Mukilteo, WA) for 24 h with a rotation speed of 60 rpm and chrome steel balls of approximately 19 mm in diameter as the grinding medium. On the other hand, paraffin wax was sliced into smaller pieces and then ground using a commercial blender. Due to the low melting temperature of wax (53.9–55.6 °C), grinding was repeated after freezing the already-ground wax to obtain finer particles. The ground wax was sieved using a stainless steel fine mesh sifter in order to obtain fine particles. Both materials were then mixed using ball milling apparatus for 2 h but without the presence of grinding media. By weight, different compositions were prepared and tested. It was found that 75–80% paraffin wax with 20–25% expanded graphite is a good range in our test and Mill's work [7], so the mixture composition used for fabricating the following samples was 80% paraffin wax – 20% expanded graphite.

Using a microscopic measurement system SOL 161 from MICRO VU (Windsor, CA) both expanded graphite and paraffin wax particle sizes were measured. It was found that both the graphite and the paraffin particles were in the range of 50–200 microns, as shown in Fig. 4. Experiments validated that this particle size range allows successful laser sintering as shown in Fig. 5(a). Coarser particles showed poor structural stability and rough surface finish as shown in Fig. 5(b).

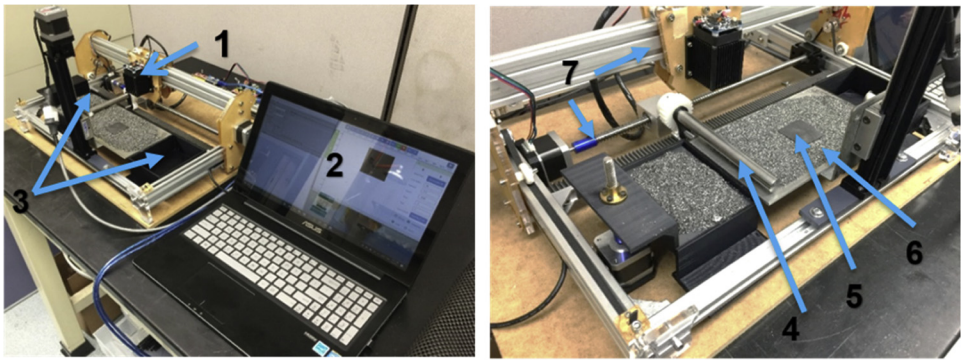

Fig. 2. Selective laser sintering setup using 5.5 W laser module, 1. Laser module 2. Computer/software, 3. Powder bins, 4. Motorized powder roller/slider, 5. Printed sample, 6. Powder bed platform (Z-stage), 7. X–Y stage.

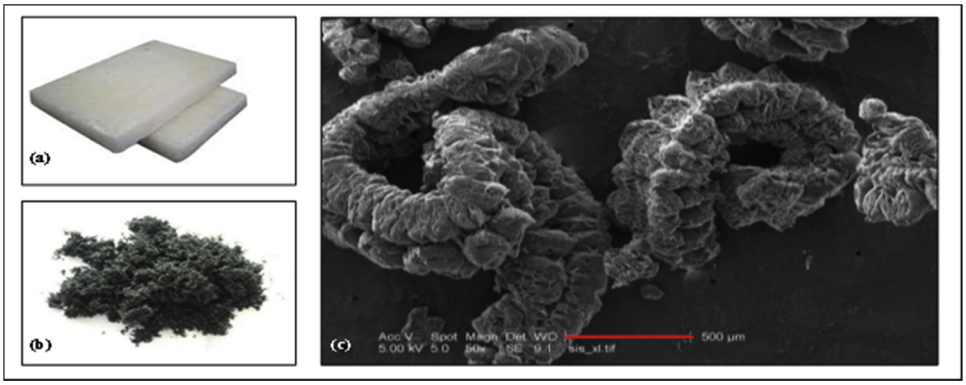

Fig. 3. (a) Paraffin wax in block form as received by the manufacturers. (b) Expanded graphite in vermicular form. (c) SEM image of expanded graphite (Superior Graphite, Chicago IL) showing the vermicular form.

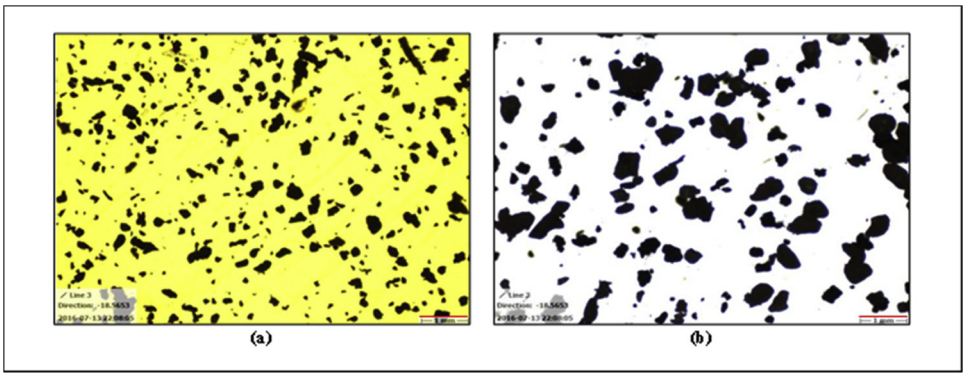

Fig. 4. (a) Microscopic images of expanded graphite particles after it has been ground using low-speed ball miller. The particle size is in the range of 50 and 200 microns. (b) Microscopic images of wax particles after it has been ground and sieved. The particle size is in the range of 50 and 200 microns.

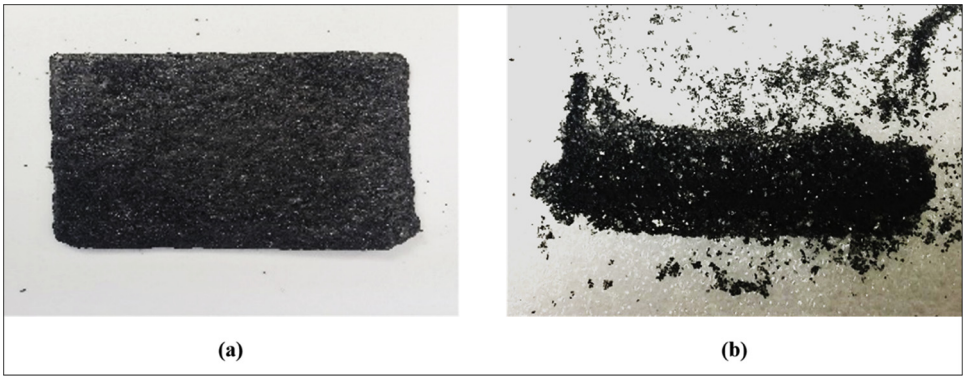

Fig. 5. (a) Sample of sintered composite trace using coarse particle size. It shows poor structural stability and rough surface finish. (b) Sample of sintered composite trace using 50–200 microns particles. It shows a much better surface finish and higher accuracy.

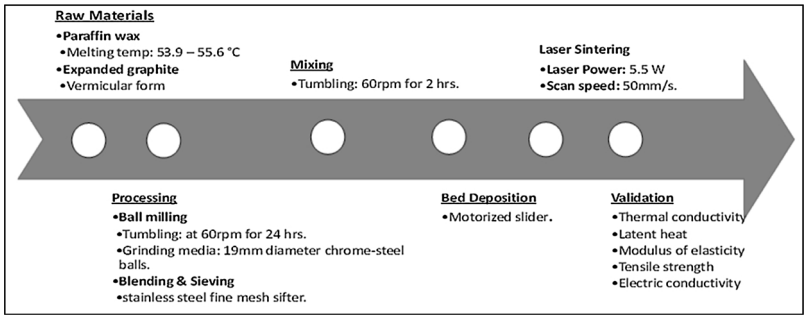

Fig. 6. Summary of the processes involved in selective laser sintering of paraffin wax/expanded graphite composite and the validation criteria.

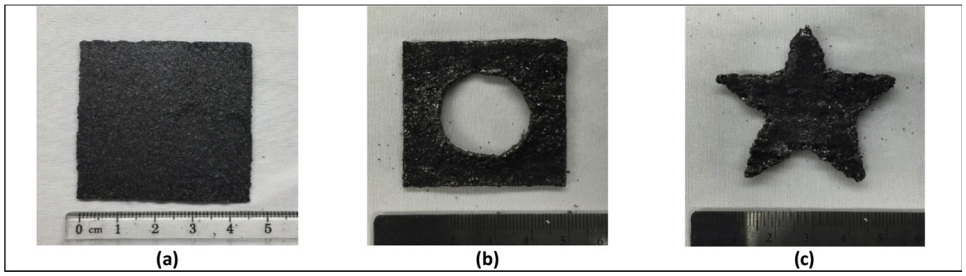

Fig. 7. Single-layer paraffin wax/expanded graphite composite samples fabricated by the developed selective laser sintering process: (a) a square sample (b) a hollow square sample; (c) a star sample.

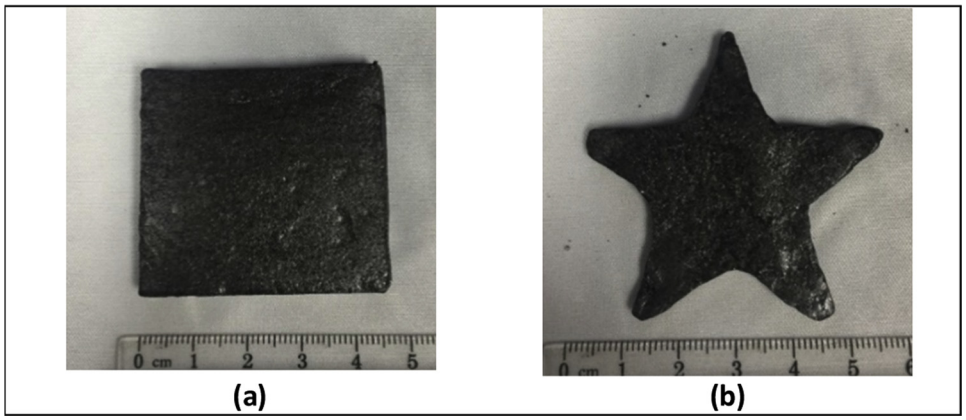

Fig. 8. Multi-layer paraffin wax/expanded graphite composite samples fabricated by the developed selective laser sintering process: (a) a square sample (b) a star sample. Layer thickness. ˜1.5 mm; loose powder thickness: ˜4 mm.

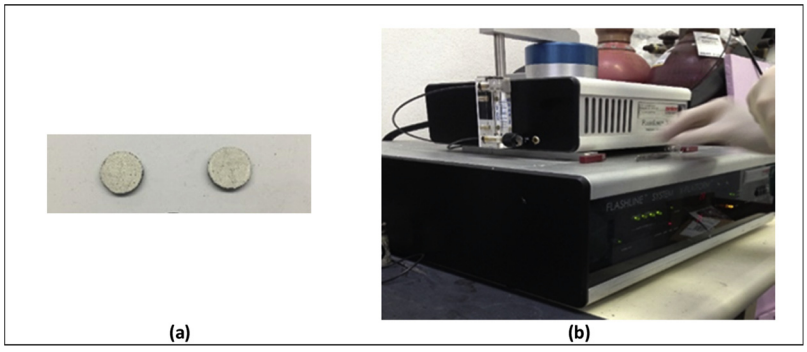

Fig. 9. (a) 12.7 mm samples with silver paint used to measure the thermal diffusivity. (b) TA Instruments DXF-200 laser flash analyzer.

Table 2
Summary of measured thermal diffusivity and thermal conductivity for 1-layer samples.

Sample No.	t (mm)	D (mm)	V (mm^3)	Avg Diff ($mm^2 s^{-1}$)	Mass (g)	Density ($g mm^{-3}$)	Cp (Jg K)	k ($W m^{-1} K^{-1}$)
1L.1.1	1.73	12.7	219.04	0.53	0.2245	0.001025	2.025	1.11
1L.1.2	1.65	12.7	208.91	0.37	0.2179	0.001043	2.025	0.78
1L.2.1	1.74	12.7	220.31	0.36	0.2165	0.000983	2.025	0.72
1L2.2	1.71	12.7	216.51	0.55	0.2167	0.001001	2.025	1.11
1L3.1	1.66	12.7	210.18	0.38	0.2185	0.001040	2.025	0.79
1L3.2	1.71	12.7	216.51	0.41	0.2171	0.001003	2.025	0.83
1L.4.1	1.87	12.7	236.77	0.31	0.2477	0.001046	2.025	0.66
1L.4.2	2.04	12.7	258.29	0.63	0.2677	0.001036	2.025	1.32

2.3. Manufacturing process

Fig. 6 describes the process of additive manufacturing of graphite-paraffin composites using selective laser sintering technique. The process starts from off-the-shelf paraffin wax and expanded graphite. A uniform mixture of graphite and paraffin particles is prepared following the procedure described in Section 2.2 for use as feedstock in the selective laser sintering process. To fabricate a 3D graphite-paraffin composite part, a flat and uniform layer of mixed expanded graphite and paraffin particles was first deposited for each layer fabrication. The computer-controlled laser module scans the surface of the powder mixture selectively to form the composite using a back-and-forth scan

Table 3
Summary of measured thermal diffusivity and thermal conductivity for 2-layer samples.

Sample No.	t (mm)	D (mm)	V (mm^3)	Avg Diff ($mm^2 s^{-1}$)	Mass (g)	Density ($g mm^{-3}$)	Cp (J g K)	k ($W m^{-1} K^{-1}$)
2L.1.1	2.01	12.7	254.49	0.41	0.2506	0.000985	2.025	0.82
2L.1.2	2.34	12.7	296.27	0.71	0.2805	0.000947	2.025	1.37
2L.2.1	2.42	12.7	306.40	0.36	0.304	0.000992	2.025	0.72
2L2.2	2.43	12.7	307.67	0.38	0.308	0.001001	2.025	0.76
2L3.1	2.5	12.7	316.53	0.35	0.2917	0.000922	2.025	0.65
2L3.2	2.74	12.7	346.92	0.51	0.3329	0.000960	2.025	1.00
2L.4.1	2.27	12.7	287.41	0.26	0.2849	0.000991	2.025	0.52
2L.4.2	2.42	12.7	306.40	0.41	0.2872	0.000937	2.025	0.77

Table 4
Summary of measured thermal diffusivity and thermal conductivity for 3-layer samples.

Sample No.	t (mm)	D (mm)	V (mm^3)	Avg Diff ($mm^2 s^{-1}$)	Mass (g)	Density ($g mm^{-3}$)	Cp (J g K)	k ($W m^{-1} K^{-1}$)
3L.1.1	2.4	12.7	303.87	0.44	0.3037	0.000999	2.025	0.90
3L.1.2	2.38	12.7	301.34	0.40	0.3034	0.001007	2.025	0.83
3L.2.1	2.66	12.7	336.79	0.52	0.3312	0.000983	2.025	1.04
3L.2.2	2.73	12.7	345.65	0.40	0.3447	0.000997	2.025	0.82
3L.3.1	2.67	12.7	338.06	0.32	0.3329	0.000985	2.025	0.65
3L.3.2	2.8	12.7	354.52	0.44	0.3453	0.000974	2.025	0.88
3L.4.1	2.97	12.7	376.04	0.65	0.2759	0.000734	2.025	0.98
3L.4.2	2.29	12.7	289.94	0.45	0.2854	0.000984	2.025	0.90

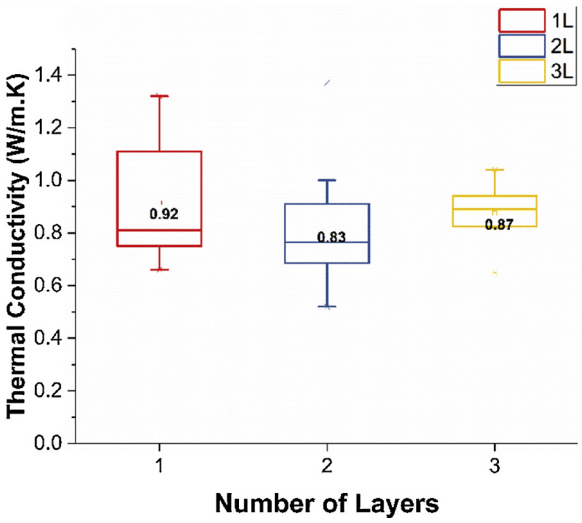

Fig. 10. Comparison of the thermal conductivity measurements of 1-layer, 2-layer, and 3-layer samples.

pattern, and a 0.25 mm scan spacing. The scan speed could be adjusted in the range of 1.5–50 mm s^{-1} to tune the laser intensity for sintering paraffin with different melting degrees and hence different impregnation capabilities. With our setup and materials, the optimal scan speed was identified as 50 mm s^{-1}, and it was used for the fabrication of the following samples discussed in Section 4. It is important to note that a lower scan speed increases the laser beam exposure, leading to an uncontrollable melting of paraffin wax and hence low accuracy. On the contrary, a higher scan speed does not provide enough laser exposure to melt all the paraffin wax particles and hence low mechanical strength and inconsistent material properties.

3. Results and discussion

3.1. Samples fabrication

With the developed testbed and prepared materials, we first fabricated and characterized single-layer samples to understand the in-layer properties of the resulted paraffin wax/expanded graphite composite as shown in Fig. 7. To validate the feasibility of fabricating a 3D multi-layer complicated structure and understand the between-layers properties, multi-layer samples with various geometries were also prepared and characterized as shown in Fig. 8. To investigate the functionalities of the produced phase change composite in thermal energy storage

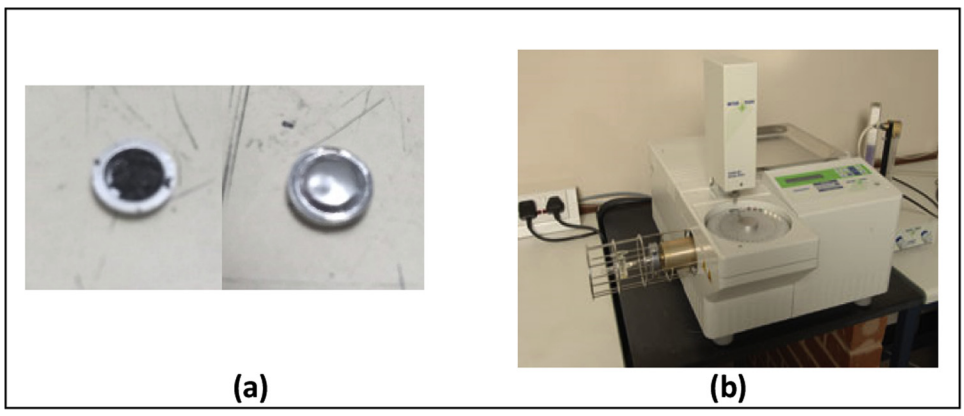

Fig. 11. (a) Sealed 40 micro-liter pan for DSC testing. (b) DSC823e/700 Mettler-Toledo differential scanning calorimeter apparatus.

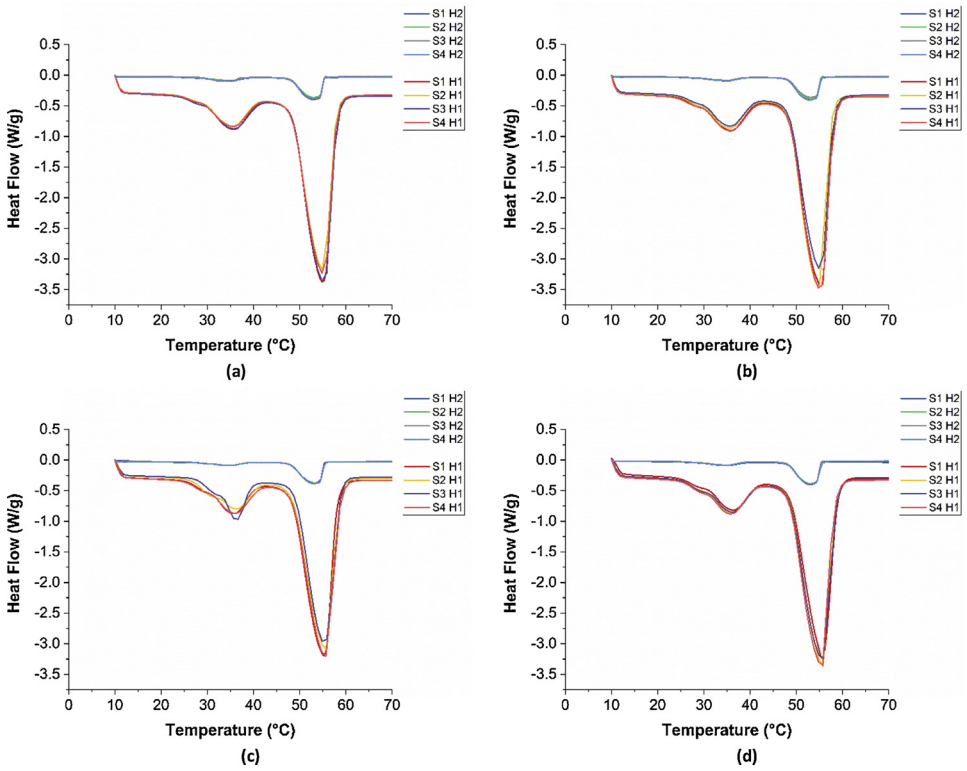

Fig. 12. Differential scanning calorimeter data of 4 samples (S1, S2, S3, S4) for 1-layer, 2-layer, 3-layer, and 4-layer samples with 2 heating rates; H1 and H2 as obtained from the apparatus, where the y-axis is heat flow in $W\,g^{-1}$, the x-axis is the temperature in °C.

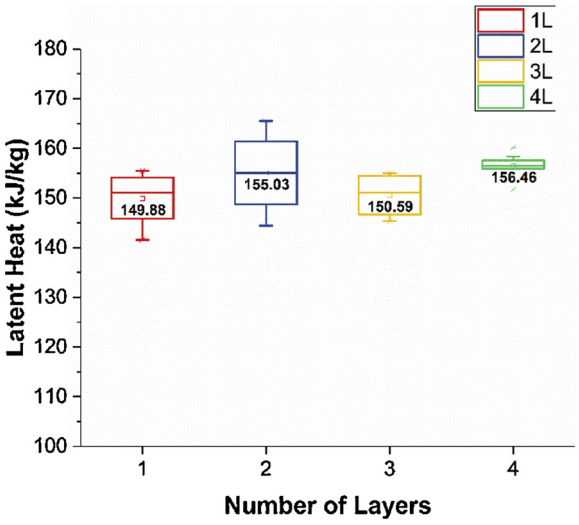

Fig. 13. Comparison of the latent heat measurements of 1-layer, 2-layer, 3-layer, and 4-layer samples.

applications, thermal conductivity, latent heat, mechanical properties, and electrical properties of 1-layer, 2-layer, 3-layer, and 4-layer samples were measured and analyzed in the following sequence.

3.2. Thermal conductivity measurements

Thermal diffusivity was measured using a laser flash analyzer DXF-200 from TA Instruments (New Castle, DE). For 1-layer, 2-layer, and 3-layer samples, two specimens were punched from the original printed samples (S1, S2, S3, S4) with a constant diameter of 12.7 mm and various thicknesses in the range of 2–3 mm as shown in Fig.9. The 4-layer samples were too thick to test due to the limitation of the laser flash analyzer, so they were excluded from thermal conductivity measurements.

To enhance the contact with the temperature sensing elements, one side was brushed with silver paint. Density was calculated, and the specific heat was estimated using the mass fraction ratio of each material as seen in Eq. (1):

$$C_p = [C_{p,EG} X_{EG}] + [C_{p,PW} X_{PW}] \quad (1)$$

where $C_{p,EG}$ and $C_{p,PW}$ are the specific heat of expanded graphite and paraffin wax respectively in ($kJ\,kg^{-1}\,K^{-1}$), while X_{EG} and X_{PW} denote the mass fraction percentage of expanded graphite and paraffin wax, respectively. The thermal conductivity, k, can be then calculated using Eq. (2):

$$k = \rho\, C_p\, \alpha \quad (2)$$

where ρ is the mass density in ($kg\,m^{-3}$), α is the thermal diffusivity in ($mm^2\,s^{-1}$). Tables 2–4 show the measured thermal conductivity results for 1-layer, 2-layer, and 3-layer samples respectively.

From Table 2, it can be seen that the thermal conductivity for 1-layer samples is in the range of 0.66–1.32 $W\,m^{-1}\,K^{-1}$ with an average of 0.92 $W\,m^{-1}\,K^{-1}$. In Table 3, the thermal conductivity for 2 layer samples is in the range of 0.52–1.36 $W\,m^{-1}\,K^{-1}$ with an average of 0.83 $W\,m^{-1}\,K^{-1}$. In Table 4, the thermal conductivity for 3-layer samples is in the range of 0.65–1.04 $W\,m^{-1}\,K^{-1}$ with an average of 0.87 $W\,m^{-1}\,K^{-1}$.

Even though the average of each case is very close to each other, the ranges differ noticeably. When the number of layers increases, the variation becomes less. This is due to the anisotropic nature of graphite particles when forming a layer structure during sintering.

Overall, sample-to-sample differences in density and thermal conductivity were observed as shown in Tables 2–4 and Fig. 10. It may be because of the variations in materials composition (paraffin wax to expanded graphite ratio), the silver painting application, and the errors in the DXF analyzer measurement.

The thermal conductivity of the 3D printed composite is lower than

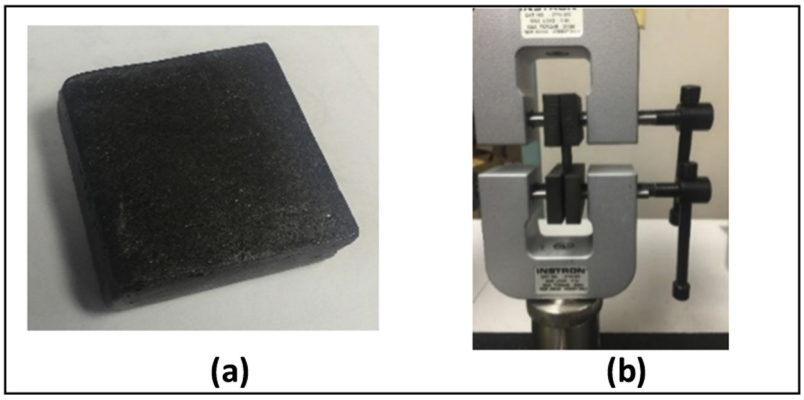

Fig. 14. (a) Mechanical tensile test specimen used testing. (b) Instron universal testing system.

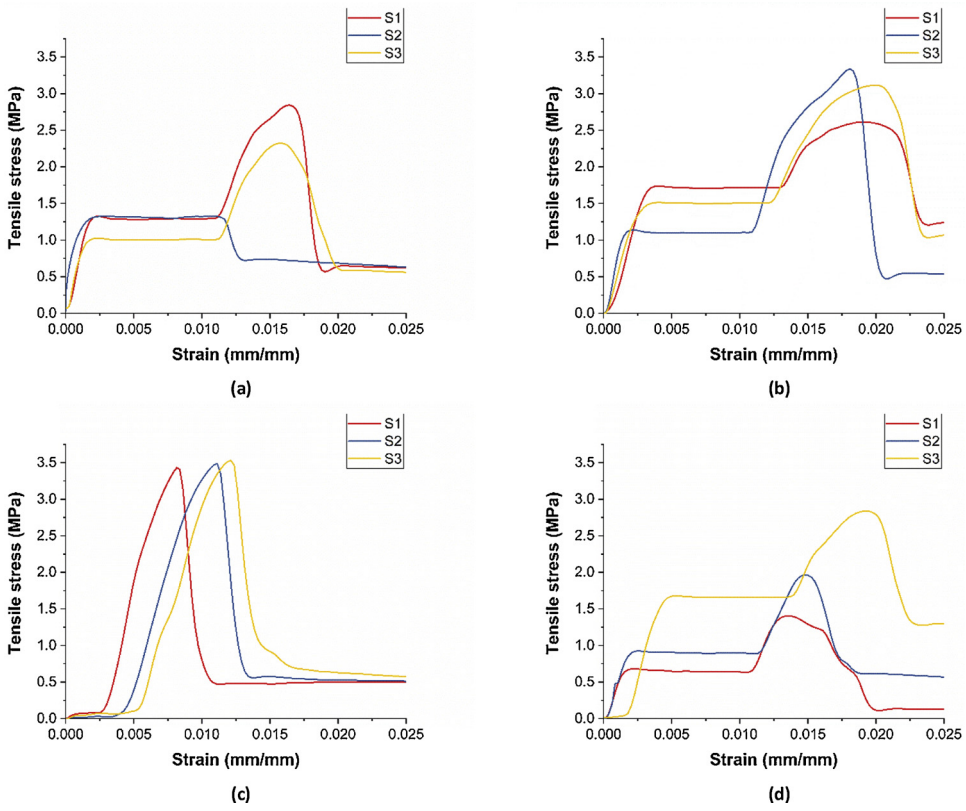

Fig. 15. Mechanical tensile testing of 3 samples (S1, S2, S3) for 1-layer, 2-layer, 3-layer, and 4-layer samples as obtained from the apparatus, where the y-axis is tensile stress in MPa, the x-axis is the mechanical strain in mm mm^{-1}.

the ones reported in the literature that fabricated by other manufacturing techniques, such as press/soak [11] and stirring [15] techniques. It is probably the molten wax in our printing process not just binds the expanded graphite particles, but some molten wax also coats the graphite particle surface. Since the paraffin wax has a very low thermal conductivity, the overall thermal conductivity of the 3D printed composite can be influenced by a small amount of wax coating on the graphite surface.

3.3. Latent heat measurements

Latent heat and phase change behaviors of the printed samples were measured using a differential scanning calorimeter (DSC) apparatus DSC823e/700 from Mettler-Toledo (Columbus, OH). In 1-layer, 2-layer, 3-layer, and 4-layer samples, two specimens were cut arbitrary from each sample (S1, S2, S3, S4) and then placed and sealed in a 40 microliter crucible as shown in Fig. 11. The test was done in two schemes: H1) heating at a temperature range of 10–100 °C at a constant ramp rate of 10 °C min^{-1}; H2) heating at a temperature range of 10–75 °C at a ramp rate of 1 °C min^{-1}. Fig. 12(a–d) shows the measured DSC results for 1-layer, 2-layer, 3-layer, and 4-layer samples respectively.

The latent heat capacity (kJ kg^{-1}) is the area under the curve of the heat flow (W g^{-1}). From Fig. 12(a), it can be seen that the latent heat for 1-layer samples is in the range of 142–155 kJ kg^{-1} with an average of 150 kJ kg^{-1}. From Fig. 12(b), the latent heat for 2-layer samples is in the range of 152–166 kJ kg^{-1} with an average of 155 kJ kg^{-1}. From Fig. 12(c), the latent heat for 3-layer samples is in the range of 145–155 kJ kg^{-1} with an average of 151 kJ kg^{-1}. Lastly, from Fig. 12(d), the latent heat for 4-layer samples is in the range of 152–160 kJ kg^{-1} with an average of 156 kJ kg^{-1}.

From Fig. 13, the averages of the latent heat capacity are relatively similar in each number of layer scenario. Unlike the thermal

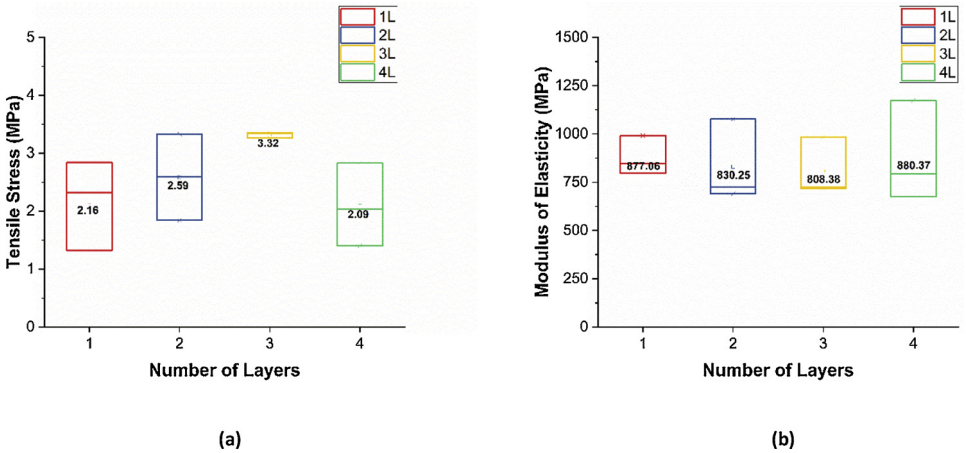

Fig. 16. Comparison of (a) tensile stress (b) modulus of elasticity measurements of 1-layer, 2-layer, 3-layer, and 4-layer samples.

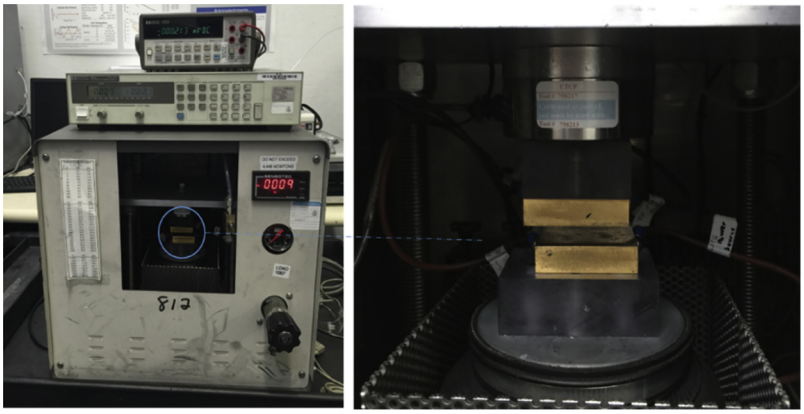

Fig. 17. Custom-built electrical resistivity measurement system.

conductivity property, latent heat capacity depends on the available weight of the phase change material – *paraffin wax in our case* – regardless of the structure of the composite. In the 4-layer samples, the range of latent heat capacities was the smallest, compared with the other number of layer scenario. This suggests that when the number of layers increases, the phase change composition becomes more uniform. Overall, since the specimens were cut arbitrary from each sample, the amount of paraffin wax may be slightly different, which explains the variation in the measurements in general. It is important to note that the pure paraffin wax that was used in this study has a latent heat capacity of ~200 kJ kg^{-1}. With 80% wax to 20% graphite ratio by weight, the composite latent capacity range suggests a successful utilization of the latent heat of paraffin wax.

3.4. Mechanical tensile measurements

Mechanical tensile tests were performed to evaluate the structural strength of the phase change composite fabricated by the proposed selective laser sintering process. Three samples of 1-layer, 2-layer, 3-layer, and 4-layer samples (S1, S2, S3) were tested at room temperature using a universal testing system 3300R from Instron (Norwood, MA) as shown in Fig. 14. An extension rate of 50 mm min^{-1} was applied. Figs. 15 and 16 show the mechanical tensile test results.

From Fig. 16, the mechanical tensile stress (S) was in the range of 2.1–3.3 MPa, while the modulus of elasticity (E) was in the range of 808–880 MPa.

Fig. 15(a, b, d) shows that the tensile samples have very brittle behavior, characterized by cracks splitting near the centerline. This observation is in agreement with the tensile test results of Alrashdan et al. [11] where the fracture happens at 90° along the tension axis, suggesting a moderate brittleness of the material.

The 3-layer samples in Fig. 15(c) shows a different trend of stress-strain curve comparing to the other samples even though the three replications (S1, S2, S3) have similar behavior. It suggests a ductile-like material behavior where the yield stress is low. This may be due to the instrument setup, the ambient conditions when the test was conducted, and variations in materials composition.

3.5. Electrical resistivity measurements

In some applications, for example, electronics packing, the electrical resistivity of the fabricated composite part is an essential property that needs to be considered. In electronics, low resistivity could potentially cause an electrical short circuit that may lead to severe hazardous. Therefore, we measured the electrical resistivity of the samples fabricated by the proposed selective laser sintering process.

The measurements of electrical resistivity were conducted using a custom-made apparatus that consists of a power source 6641A and a Multimeter 34401A from Hewlett Packard (Palo Alto, CA) as shown in Fig. 17. To minimize the contact resistance during measurements, the sample was sandwiched between gold-plated metal leads, using a custom-built compression apparatus. Electrical resistivity is then calculated. Fig. 18(a–d) shows results for 1-layer, 2-layer, 3-layer, and 4-layer samples respectively.

As shown in Fig. 18, the paraffin wax/expanded graphite composite fabricated by the proposed SLS process have very low electrical conductivity, compared with the expanded graphite, which can reach up to 4×10^5 S m^{-1} depending on the orientation of the carbon chain

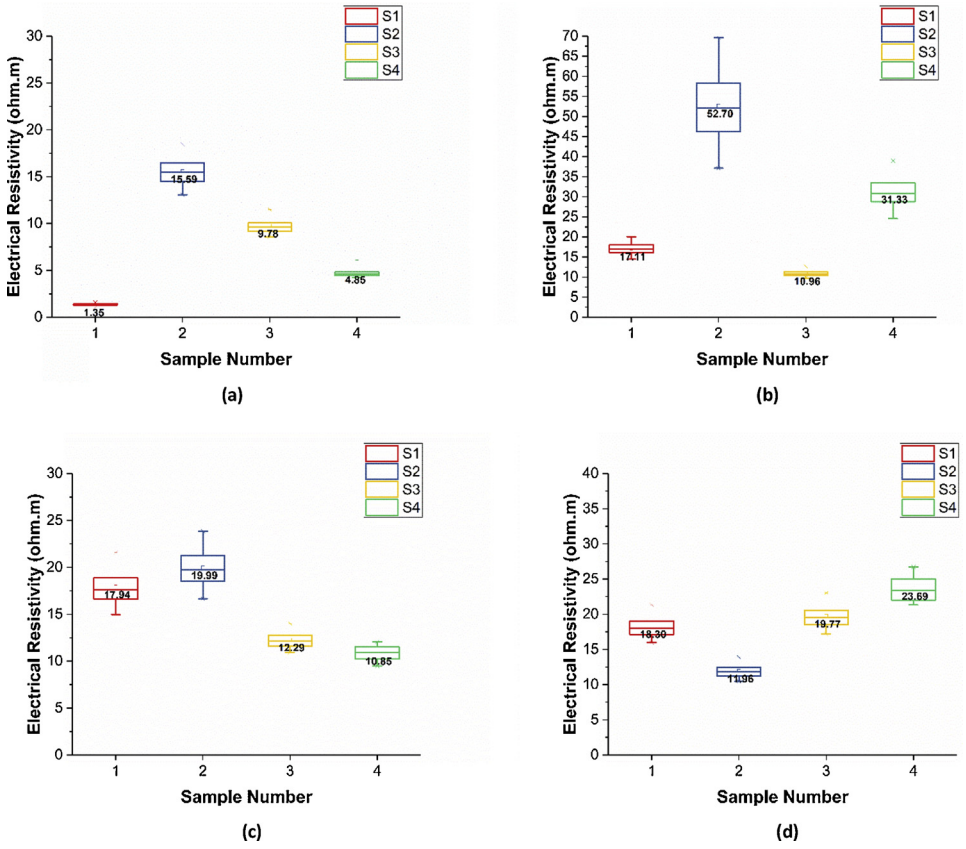

Fig. 18. Electrical resistivity measurements of 4 samples (S1, S2, S3, S4) for 1-layer, 2-layer, 3-layer, and 4-layer samples.

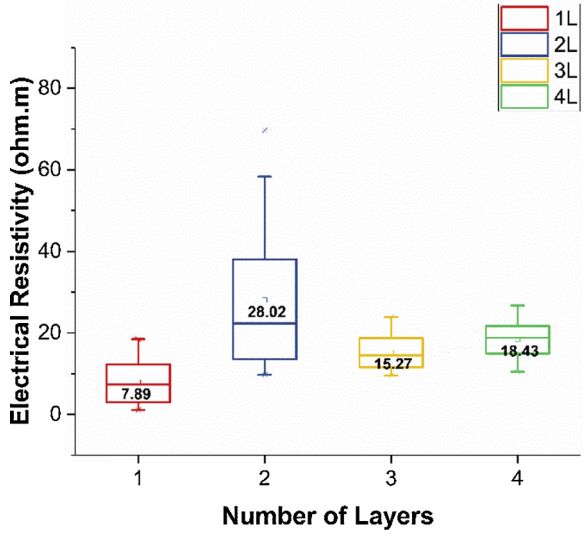

Fig. 19. Comparison of the electrical resistivity measurements for 1 layer, 2 layers, 3 layers, and 4 layers samples.

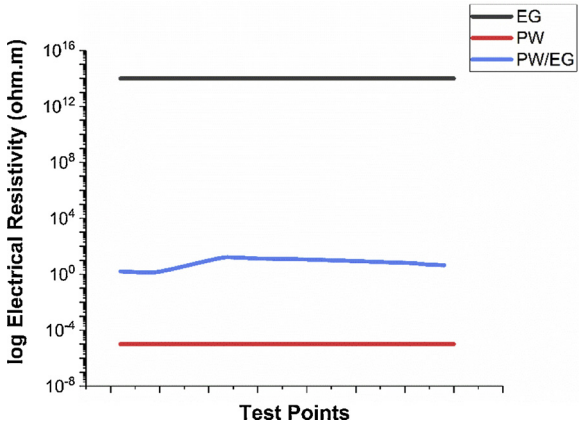

Fig. 20. Electrical resistivity ranges for expanded graphite (EG), paraffin wax (PW), and the fabricated paraffin wax/expanded graphite composite (EG/PW) in log scale (ohm m).

structure [13]. Since the composite has 80% paraffin wax by weight, this indicates that the paraffin wax, which can be considered as an electric insulator with an electrical conductivity as low as 1×10^{-15}–10^{-13} S m^{-1}, has a dominant effect in determining the electrical conductivity of the 3D printed composite, as shown in Fig. 20.

In Fig. 19, the variations in the electrical resistivity measurements could be due to the high sensitivity of the multimeter used, and the sample's surface finish that affects the contact resistance between the gold-plated metal leads and the ambient conditions. It can be noted that when the number of layers increases, the variation becomes less (3-layer and 4-layer samples). This observation aligns with the other properties measurements (thermal conductivity and latent heat) where the variation within becomes less when the number of layers increases.

3.6. Discussion

To summarize, Table 5 shows a comparison between the developed SLS process and other fabrication approaches for the production of paraffin wax/expanded graphite composites that were reported in the literature in terms of manufacturing capability, thermal, mechanical, and electrical properties of fabricated parts.

The paraffin wax/expanded graphite phase change composite fabricated by selective laser sintering technique showed a moderate

Table 5
Comparison between the SLS process developed in this study and other reported fabrication methods.

Method	Ratio	ρ	k	Δh	S	E	α	Processing time	
	PW/EG %	kg m^{-3}	W m^{-1} K^{-1}	kJ kg^{-1}	MPa	MPa	ohm m	As reported	min cm^{-3}
Mixing-based [14]	85.6/14.4	715.7	–	161.4	–	–	–	250 min/ g of EG	26
Stirring-based [15]	80/20	–	7.65	141.7	–	–	–	–	–
Impregnation-based [4]	90/10	721	0.82	178.3	–	–	–	60 min until saturation	60
Press & soaking-based [11]	80/20	789	14.3	–	1.04	–	–	720 min until saturation	6
SLS-based	80/20	860	0.9	155	2.5	850	20	4.85 min for 50 × 50 × 2 mm	< 1

thermal conductivity, good latent heat, and form-stable structural integrity, comparing with the existing phase change materials used in the thermal energy storage market. In addition, it showed a very low electrical conductivity, which is a very critical aspect when used in electronics. Furthermore, the proposed SLS technique demonstrates a much shorter build time, comparing with other methods, such as the conventional "pressing soaking" method. The conventional "days" build time of paraffin wax/expanded graphite composite product now can be reduced to "hours" by using the proposed SLS method. In addition, the capability of SLS on forming freeform structures without any post drilling or machining further shortens the time-to-market and saves a significant amount of material that would be wasted in conventional manufacturing systems.

4. Conclusions

In this paper, a novel method for fabricating expanded graphite/paraffin wax phase change composite was explored and a proof-of-concept laser sintering setup was constructed. To achieve successful sintering, paraffin wax particles and expanded graphite particles with a diameter in the range of 50–200 microns were prepared. Various single-layer and multi-layer samples were fabricated by using the prepared materials and the developed SLS process. The thermal conductivity of the sintered composite was found to be in the range of 0.83–0.92 W m^{-1} K^{-1}. The latent heat of the sintered composite was measured using DSC and it was found to be in the range 150–156 kJ kg^{-1}. In addition, the ultimate tensile strength of the sample produced by the developed laser sintering process was in the range of 2.2–3.3 MPa and the average Modulus of elasticity was between 808–880 MPa. Finally, the electrical resistivity is in the range of 8 and 28 Ohm m, which is highly influenced by the paraffin wax insulation property. The effectiveness and efficiency of the SLS process in fabricating paraffin wax/expanded graphite phase change composite for thermal energy storage applications have been validated.

Future work will focus on the fabrication of multi-layer paraffin wax/expanded graphite composite structures with improved dimensional accuracy, surface finish, and enhanced thermal conductivity.

Acknowledgment

Special thanks to AllCell Technologies (Chicago, IL) for the support of this work.

References

[1] Py X, Olives R, Mauran S. Paraffin/porous-graphite-matrix composite as a high and constant power thermal storage material. Int J Heat Mass Transf 2001;44(14):2727–37.
[2] Sears FW, Zemansky MW, Young HD. University physics. Addison-Wesley; 1987.
[3] Sarı A. Form-stable paraffin/high density polyethylene composites as solid–liquid phase change material for thermal energy storage: preparation and thermal properties. Energy Convers Manage 2004;45(13):2033–42.
[4] Sarı A, Karaipekli A. Thermal conductivity and latent heat thermal energy storage characteristics of paraffin/expanded graphite composite as phase change material. Appl Therm Eng 2007;27(8):1271–7.
[5] Fang X, Fan LW, Ding Q, Yao XL, Wu YY, Hou JF, et al. Thermal energy storage performance of paraffin-based composite phase change materials filled with hexagonal boron nitride nanosheets. Energy Convers Manage 2014;80:103–9.
[6] Ouyang T, Chen Y, Xie Y, Yang K, Bao Z, Zhong J. Thermal transport in hexagonal boron nitride nanoribbons. Nanotechnology 2010;21(24):245701.
[7] Mills A, Farid M, Selman JR, Al-Hallaj S. Thermal conductivity enhancement of phase change materials using a graphite matrix. Appl Therm Eng 2006;26(14):1652–61.
[8] Khateeb SA, Farid MM, Selman JR, Al-Hallaj S. Design and simulation of a lithium-ion battery with a phase change material thermal management system for an electric scooter. J Power Sources 2004;128(2):292–307.
[9] Mills A, Al-Hallaj S. Simulation of passive thermal management system for lithium-ion battery packs. J Power Sources 2005;141(2):307–15.
[10] Celzard A, Mareche JF, Furdin G. Modelling of exfoliated graphite. Prog Mater Sci 2005;50(1):93–179.
[11] Alrashdan A, Mayyas AT, Al-Hallaj S. Thermo-mechanical behaviors of the expanded graphite-phase change material matrix used for thermal management of Li-ion battery packs. J Mater Process Technol 2010;210(1):174–9.
[12] Guo N, Leu MC. Effect of different graphite materials on the electrical conductivity and flexural strength of bipolar plates fabricated using selective laser sintering. Int J Hydrogen Energy 2012;37(4):3558–66.
[13] Pierson HO. Handbook of carbon, graphite, diamonds and fullerenes: processing, properties and applications. William Andrew; 2012.
[14] Zhang Z, Fang X. Study on paraffin/expanded graphite composite phase change thermal energy storage material. Energy Convers Manage 2006;47(3):303–10.
[15] Wu W, Zhang G, Ke X, Yang X, Wang Z, Liu C. Preparation and thermal conductivity enhancement of composite phase change materials for electronic thermal management. Energy Convers Manage 2015;101:278–84.